



An investigation of sea level and circulation response during a coastal trapped wave event on the Eastern Agulhas Bank, South Africa

Dylan F. Bailey^{a,b,c,*}, Juliet Hermes^{b,c}, Pierrick Penven^d, Thomas G. Bornman^{b,c}, Wayne Goschen^c

^a Bayworld, Port Elizabeth Museum, Port Elizabeth, South Africa

^b South African Environmental Observation Network, Elwandle and Egagasini Nodes, South Africa

^c Institute for Coastal and Marine Research, Nelson Mandela University, Port Elizabeth, South Africa

^d University of Brest, CNRS, IRD, Ifremer, Laboratoire d'Océanographie Physique et Spatiale, IUEM, France

ARTICLE INFO

Keywords:

Coastal trapped wave
Regional ocean modelling system
Wind event
Agulhas bank
Algoa bay
Numerical ocean model

ABSTRACT

Coastal trapped waves (CTW) have the potential to capture and transport a significant amount of energy from atmospheric wind systems, in turn inducing sudden changes to the coastal marine environment over large areas, even those remote to the propagating wind system. In this study, the effects of a large, eastward travelling CTW that was captured on *in situ* moored acoustic doppler current profiler (ADCP) (~30 m bottom depth) and sea level recording instrumentation in Algoa Bay on the eastern Agulhas Bank off South Africa is examined using a high-resolution (dx~1 km) Regional Oceanographic Modelling System (ROMS) ocean model. Alongshore current reversals to the full depth were seen in both the model and two ADCP moorings as the CTW traversed the study domain, with strong currents exceeding 1 m/s developing directly to the south of Cape St Francis and Cape Recife at the peak of the event within the model. In a special model run with surface wind stresses removed, it was shown that the CTW carries much of the energy into the domain from remote wind forcing to the west, contributing an estimated 82% of the eastward flux of shelf water. The total volume of water displacement during the CTW was estimated at $335.2 \times 10^9 \text{ m}^3$ which balanced (completion of a full wave cycle) over a period of 150h after the initial zero-crossing point of the transport flux.

1. Introduction

Coastal trapped waves (CTW) are a regular feature along shelf regions, presenting as sub-inertial waves typically initiated by wind stress and propagating along coastal boundaries with characteristics of Kelvin waves, continental shelf waves, and edge waves (Adams and Buchwald 1969; Gill and Schumann 1974; Huthnance 1975; Gill 1982).

Along the coast of South Africa, CTW were first described by Gill and Schumann (1974). Schumann and Brink (1990) assessed air pressure, tide level recorders, and currents to further characterize CTW off the south coast of South Africa, and found that CTW commonly occur here as lowest mode barotropic shelf waves with periods within the weather band of between 3 and 20 days and phase propagation speeds anywhere from 4.4 to over 9 m/s. These figures were similar to that found by Maiwa et al. (2010) and Woodham et al. (2013) for CTW on the Australian south coast, with periods between 10 and 25 days and propagation speeds from 3.4 m/s to over 10 m/s. Schumann and Brink

(1990) noted that conditions of near resonance between wind systems and CTW can exist along the South African south coast, which was confirmed by Jury et al. (1990), leading to the formation of large waves sometimes exceeding 50 cm in amplitude. These large CTW can have profound, although short lived effects on the regional ocean state and can be a considerable contributor to near shore variability (e.g. Tilney et al., 1996; Schumann 1999). Data analysed from Acoustic Current Doppler Profilers (ADCP), deployed by Goschen et al. (2012) off Woody Cape in the north-eastern sector of Algoa Bay, one of two large crenulated bays on the south-eastern section of the Agulhas Bank, show that currents here are influenced by CTW passing through this region, causing periodic reversals in current flow. CTW are not a regularly observed feature off the south-east coast far north of East London (Schumann 1983), attributed to the dissipation of the waves as they travel eastward past Algoa Bay along the narrowing shelf and interact with the fast south-westward flowing Agulhas Current (AC) (Brink 1990, 2006).

* Corresponding author. Bayworld, Port Elizabeth Museum, P.O. Box 13147, Humewood, Port Elizabeth, 6013, South Africa.

E-mail address: dylan.bailey@bayworldoceanarium.com (D.F. Bailey).

<https://doi.org/10.1016/j.csr.2022.104698>

Received 15 April 2021; Received in revised form 4 March 2022; Accepted 5 March 2022

Available online 8 March 2022

0278-4343/© 2022 Elsevier Ltd. All rights reserved.

Gaining a better understanding of the role that CTW play in the coastal environment is becoming ever more critical in a rapidly changing climate where coastal communities and natural marine habitats are exposed to intensifying transient environmental events. The risk of flooding and infrastructure damage along the South African coastline due to sea level rise and storms is increasing (Lück-Vogel et al., 2019), with an estimated 24 552 buildings and 57 922 people falling within the medium to high coastal risk class. A large percentage (60%) of coastal settlements also fall within this category, with many high-risk settlements found along the south coast where the largest amplitude CTW are known to propagate (Jury et al., 1990; Schumann and Brink 1990). In addition to infrastructure, it is also critical to understand the impact of CTW events on food security. For example, work done along the south coast of South Africa has shown the importance of eastward displacement of larval fish stages in transporting them from spawning to nursery grounds (Brouwer et al., 2010), but also has the potential of moving them out of marine protected areas (MPA) (Roberts 2010; Patrick et al., 2013). Estuaries are also important nursery and spawning areas for many fish species, the variability of which is greatly influenced by CTW, as shown by Schumann (2013). Although described in the local context here, environmental change impacts are a global concern (Pörtner et al., 2019).

Several studies have employed ocean models to detail the regional specific characteristics, propagation, and forcing mechanisms of CTW (Martínez and Allen 2004a, 2004b; Maiwa et al., 2010; Ding et al., 2012; Woodham et al., 2013; Bachèlery et al., 2020). A limited number of these have applied high spatial ($dx < 12$ km) and temporal ($dt < 12$ h) resolution regional ocean model outputs to further interrogate the propagation characteristics of CTW (for example, Martínez and Allen 2004a; 2004b; Ding et al., 2012). However, apart from a dissertation by Nhantumbo (2014), there has been no application of high resolution ocean models to furthering the understanding of CTW along the coastal region of the Agulhas Bank. While much work has been done with respect to both the general and regional characteristics of CTW globally, when considering the often drastic responses in the coastal environment to their passage, the readily available access to high performance ocean models provides opportunities to build on current understandings of CTW behaviour by detailing unique, location-specific transient changes induced by these phenomena. Presented as a case study, a realistically forced, high resolution ($dx \sim 1$ km, $dt = 3$ h) configuration of the Regional Ocean Modelling System (ROMS) is used to examine the effects of a large amplitude CTW on water circulation and displacement as it progresses along the coastal region of a narrowing shelf and passes two adjacent bays on the eastern sector of the Agulhas Bank, namely St Francis Bay and Algoa Bay.

2. Data and methods

2.1. Study area

The region of focus is the eastern Agulhas Bank, found on the south-eastern portion of the southern African continental shelf (Fig. 1), with the study domain extending from Oyster Bay to north of Port Alfred (locations relative to the southern coast shown in Fig. 4), outlined in Fig. 1b. The shelf here has an average depth of 120 m and progressively narrows to the north-east, from 50 km off Cape St Francis to 34 km off Port Alfred (measured from the coast to the 200 m isobath), bounded by a coastline to the north and a steep shelf break to the south that descends rapidly to beyond 1000 m depth. The shelf break is flanked by the Agulhas Current, a major western boundary current that follows the continental shelf break on the east coast of southern Africa with a typical width of 70–90 km, a depth of 2300 m, and a surface core velocity often exceeding 2.5 m/s (Roberts et al., 2010), with a mean southward transport of between 77 and 84 Sv (Beal et al., 2015). Two large crenulated bays are found near 34°S, Algoa Bay and St Francis Bay. Algoa Bay is relatively shallow, not exceeding 70 m in depth (Bremner 1983).

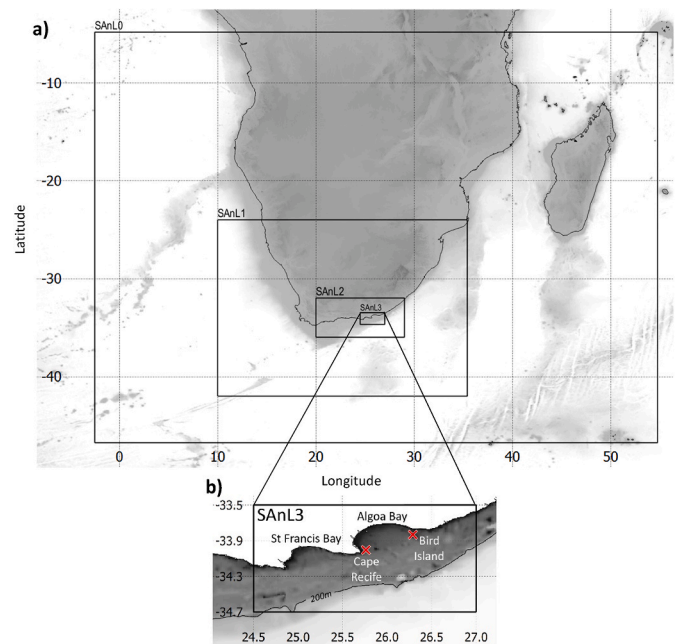


Fig. 1. (a) Relative position of the model domains, outlined by solid black lines, with respect to the sub-Saharan African and Madagascan continent. (b) Extents of SANL3 model domain from Oyster Bay to north of Port Alfred, encompassing St Francis Bay and Algoa Bay, used in this study, with the locations of the SAEON ADCP and UTR moorings at Cape Recife and Bird Island. Latitude and longitude in decimal degrees. Shelf to the 200m isobath denoted by dark shaded area, with 200m isobath shown in (b).

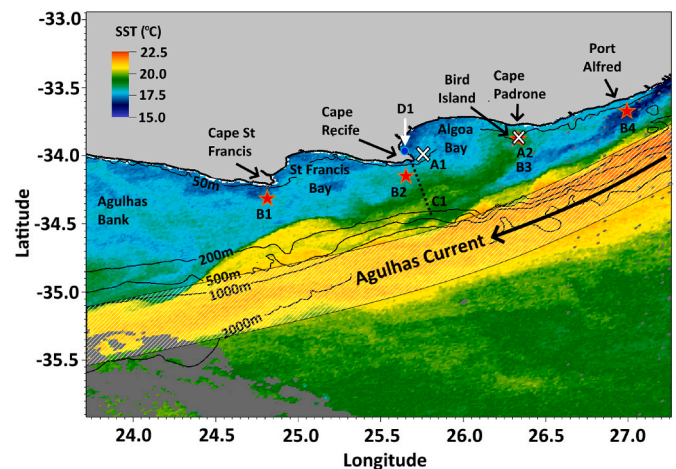


Fig. 2. MODIS sea surface temperature (SST) image taken on 21 July 2009 with bathymetry overlay of the south eastern coast of South Africa off Algoa Bay to illustrate the typical path of the warm (>21 °C) Agulhas Current as indicated off the continental shelf margin. White crosses denote locations of Cape Recife (A1) and Bird Island (A2) ADCP moorings. Red stars denote locations of the Cape St Francis (B1), Cape Recife (B2), Bird Island (B3) and Port Alfred (B4) locations used for current assessments in the numerical models. Dashed line denotes transect used for volume transport assessment (C1). Location of the SANHO Tide Recorder at the Port Elizabeth Harbour shown by blue dot (D1). The Port Elizabeth SAWS weather station at the Port Elizabeth Airport is approximately 3 km inland of the Port Elizabeth Harbour.

A study involving ship transects and vertical profiling instruments by Goschen and Schumann (1988) demonstrated that wind and the AC are the primary driving forces behind circulation patterns within the bay. Under typical circumstances, in the absence of other forcing, surface currents within the bay and the adjacent inner shelf region tend to align

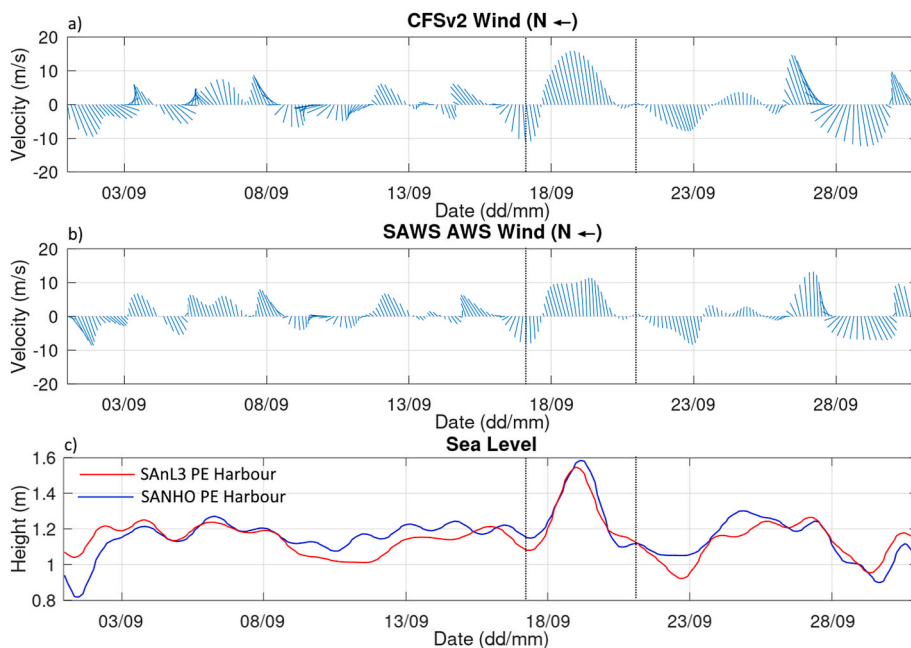


Fig. 3. (a) Wind plot from the CFSv2 dataset extracted at the SAWS AWS location at the Port Elizabeth airport. (b) Wind plot from the SAWS AWS at the Port Elizabeth airport. (c) Uncorrected sea surface height from the SANHO tide recorder at the Port Elizabeth (PE) harbour (blue) and the closest grid cell in the SANL3 reference model (red). Dates shown from 1 to 30 September 2014. Coastal trapped wave event between 17 and 22 September 2014 highlighted with dashed lines. Date lines denote midnight.

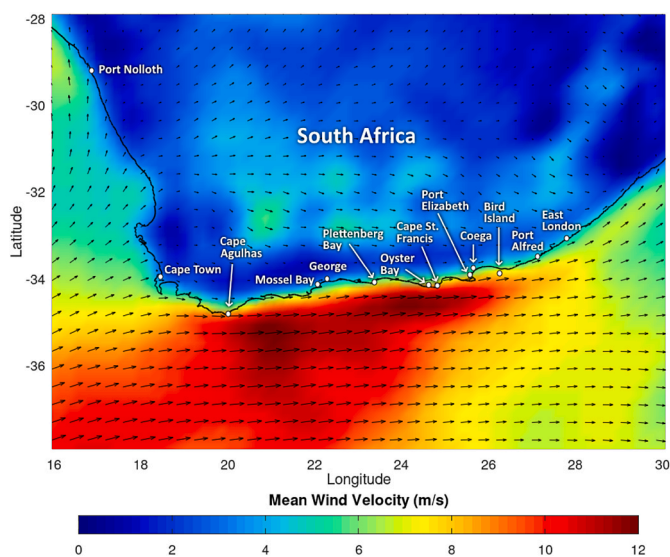


Fig. 4. Mean CFSv2 10m wind field during the westerly wind event from 12h00 17 September 2014 to 12h00 20 September 2014. Shading denotes wind velocity. Vector arrows denote wind direction. Coastal locations referenced in the text and tables shown.

to the direction of the prevailing wind, modified by the topography and the shape of the coast (Schumann et al., 2005; Roberts 2010; Patrick et al., 2013). There is little published on the oceanographic conditions of St Francis Bay. Work done by Harris (1978) showed dominant surface currents in the bay to be somewhat similar to Algoa Bay, albeit stronger and more polarised in the eastward/westward direction.

2.2. Numerical model

The Regional Ocean Modelling System (ROMS), a split-explicit, terrain following regional oceanographic model using a third-order, upstream-biased advection scheme (Shchepetkin and McWilliams 2005) was used for the three-dimensional numerical simulations. To resolve fine scale coastal circulation while considering larger mesoscale

dynamics, a multi-nested downscaling technique was employed to resolve disparities in spatial and temporal scales. A one-way, offline method of model nesting to finer scale was used without feedback from the child grid solutions (Penven et al., 2006b). The offline nesting approach used 2D boundary forcing files due to storage constraints, and thus did not employ any form of volumetric nudging. The open boundary condition (OBC) configuration was based on those used by Penven et al. (2006a), Mason et al. (2010) and Marchesiello et al. (2001) for offline regional ocean model nesting. For the ROMS configuration described here, prognostic variables were connected to the external conditions in the open boundary configurations using Orlandi active radiation schemes for the baroclinic mode (for both temperature and salinity), and modified Flather-type characteristic radiation scheme for the barotropic mode (Marchesiello et al., 2001). A baroclinic velocity nudging coefficient ($M3$) of 0.05 day^{-1} was used for inflow and 0.05 day^{-1} for outflow. A total of four regional model domains, a parent and three child nests, were defined on an Arakawa-C Mercator grid, hereafter referred to as SANL0, SANL1, SANL2, and SANL3 respectively (Fig. 1). Child grids were nested in a one-way and offline configuration using a downscaling factor of 3. Domain specific configurations, including time frames for surface forcing, lateral boundary inputs and spin up are summarised in Table 1. SANL0 was the parent grid, providing lateral climatological boundary conditions for the first nest SANL1. Lateral boundary conditions for SANL2 and SANL3 were then interpolated from the outputs of the prior nest. All grids and forcing files were created using ROMSTOOLS (https://www.croco-ocean.org/download/roms_agrif-project/), a toolbox of Matlab scripts and datasets that aid in the configuration of grids and production of forcing files for ROMS. Additional Matlab code was used from the ROMS Numerical Toolbox (<http://oces.us/RNT/>) to produce the offline lateral boundary conditions between nested grids.

Ocean and atmospheric biases in coupled OGCM simulations have recently received greater attention thanks to the broad range of readily available model data from in the Coupled Model Intercomparison Project (CMIP) (for examples relating to the Indian Ocean, see Tao et al., 2016; and Shikha and Valsala, 2018). Given the inherent sensitivity of the Agulhas current to the dynamics of the equatorial region of the Indian Ocean in ocean models (see Hermes et al., 2007; Backeberg et al., 2008; Durgadoo et al., 2013; Hutchinson et al., 2018), an approach was considered to reduce the introduction of potential biases should the

Table 1
Nested domain configurations for ROMS.

	SAnL0	SAnL1	SAnL2	SAnL3
Domain	2.5° W -	10.0° E -	20.0° E -	24.5° E -
Extents	54.75° E; 4.8° S - 46.75° S	35.4° E; 24.0° S - 42.0° S	29.0° E; 32.0° S - 36.0° S	26.5° E; 33.7° S - 34.7° S
Domain Resolution	1/4° (~28 km)	1/12° (~9 km)	1/36° (~3 km)	1/108° (~1 km)
Surface Forcing	NCEP CFSv2	NCEP CFSv2	NCEP CFSv2	NCEP CFSv2
Bulk Flux Forcing Time	6 h	6 h	6 h	6 h
Surface Wind Stress Forcing Time	6 h	6 h	1 h	1 h
Lateral Boundary Forcing	WOA05	SAnL0	SAnL1	SAnL2
Lateral Boundary Time	Monthly	Daily	8 h	3 h
Tides Enabled	No	No	No	Yes
Spin Up Period	5 years	3 years	1 year	1 year
Output Time	Daily	8 h	3 h	3 h

boundaries had been forced from such an inter-annual OGCM model. To this end, the parent domain, SAnL0, used a modified SAFe configuration (Penven et al., 2006a), where the surface was forced using an inter-annual atmospheric dataset and the lateral boundary conditions forced using the Levitus, Sydney; US DOC/NOAA/NESDIS (National Oceanographic Data Center, 2013) monthly climatology. A full evaluation was carried out to ensure that the parent SAnL0 model was of a suitable size and resolution to resolve the most important of the basin scale processes at the correct time scales for the subsequent nests (Bailey 2020).

A surface forcing atmospheric dataset with hourly wind variables was chosen in order to resolve fine temporal scale coastal ocean circulation as accurately as possible (Cucco et al., 2019). The NCEP Climate Forecast System version 2 (CFSv2) (Saha et al., 2014) provided historical hourly timeseries analysis over the required time period on a 0.205° by 0.205° global grid and was used to surface force the SAnL0, SAnL1, SAnL2, and SAnL3 reference domains. Tides were only enabled for the SAnL3 domain, forced from the lateral boundaries using the M2, S2, N2, K2, K1, O1, P1, Q1, Mf, and Mm tidal components from the TPXO7 global ocean tide model dataset (Egbert and Erofeeva 2002). The 30 arc-second GEBCO_2014 gridded dataset (version 20150318, www.gebco.net) provided the bathymetric data for all domains. This was bilinearly interpolated onto the grid and smoothed with an r-factor of 0.2 to reduce pressure gradient errors (Haidvogel and Beckmann 1999). All model domains had 42 vertical σ -coordinate levels with surface and bottom grid nonlinear stretching factors of $\theta_s = 6$ and $\theta_b = 0$, respectively (Shchepetkin and McWilliams 2005). Models were run in a free slip configuration using a split and rotated 3rd order upstream biased advection scheme (Marchesiello et al., 2009). The integration period was five years, spanning from 1 January 2011 to 31 December 2015, with average outputs (of all model time steps over the sampling period of the output) of temperature, salinity, and momentum (sampling periods shown on Table 1). Models were spun up by repeating the 2011 forcing year as many times as needed to obtain statistical equilibrium (shown in Table 1).

2.3. Observation data

In situ current data was obtained from the South African Environmental Observation Network (SAEON) Acoustic Doppler Current Profiler (ADCP) instrument moorings located at Cape Recife (Fig. 2: A1) and

Bird Island (Fig. 2: A2) at the eastern and western ends of Algoa Bay respectively. Sea level data was obtained from the South African National Hydrographers Office (SANHO) Tide Recorder located at the Port Elizabeth Harbour in Algoa Bay (Fig. 2: D1), as well as Port Nolloth, Cape Town, Mossel Bay, Knysna, and East London. Weather data was obtained from the South African Weather Services (SAWS) Automatic Weather Stations (AWS) at Cape Agulhas, Plettenberg Bay, Port Elizabeth, Coega, Bird Island, Port Alfred and East London (Fig. 4).

2.4. Identification of event for the case study

To simplify the search for a potential CTW event, tide level records were first compared and correlated with sea level changes and wind. Considering that the strongest responses are to be found in near resonant conditions (Clarke and Brink 1985), propagating wind systems travelling east along the south coast that maintained significant wind speeds during their passage were examined. Only a few strong southwesterly wind events occurred in the time period of the model that provided optimal conditions for an assessment. Additionally, the Agulhas Current (AC) should not be in a meandering state and should be free of cyclonic eddy activity (eg. Lutjeharms and Roberts 1988; Schumann and van Heerden 1988; Lutjeharms et al., 2003a; 2003b) (confirmed by visual inspection of sea surface temperature (SST)) in both the numerical model and *in situ* environment, and ADCP and Tide Recorder data should be available for that time. Only a single wind system propagating through the study region between 17 and 20 September 2014 (Fig. 3) met these requirements. It was also the only significant southwesterly wind event to occur for that month.

2.5. Sea level, alongshore currents, and along-shelf transport assessment

Four key locations in the model located within 6 km of the shoreline (Fig. 2 red stars: south of Cape St Francis (B1) (65 m depth), Cape Recife (B2) (55 m depth), and Bird Island (B3) (35 m depth), and southeast of Port Alfred (B4) (30 m depth)) were used to assess sea level and alongshore currents during the event. Along-shelf volume transport (assessed by depth-integration of flow across a transect) was measured between Cape Recife and 10 km inshore of the mean position of the AC inshore front to reduce interference from any submesoscale ($O < 10$ km) frontal variability (Fig. 2 dashed line: C1) (Lutjeharms et al., 1989; Krug et al., 2017; Tedesco et al., 2019).

The influence of remote forcing to the west of the western domain boundary at Oyster Bay on the circulation on the shelf and bays during the event was assessed by comparing the SAnL3 reference model (forced with surface winds from CFSv2) with a modified SAnL3 model run where all surface wind forcing was removed while maintaining advective surface heat fluxes. Shelf waves and edge waves (CTW) and currents were free to pass through the domain in this configuration, but with no further input of kinetic energy from local wind forcing.

Unless otherwise stated, all sea level plots were low-pass filtered to daily values using a Lanczos filter with a quarter-power point of 32.26 h, a compromise derived through experimentation to reduce the diurnal tidal signal while retaining short term variations caused by the passing wind system. Data for all wind stick plots was smoothed using a Lanczos low-pass filter with a quarter-power point of 28.5 h, as done by Goschen et al. (2012), and averaged to 3 h to match *in situ* and model time steps. Sea level correction along the south coast was done for Port Elizabeth, using air pressure (Gaspar and Ponte 1997) from the AWS at the Port Elizabeth Airport, and Mossel Bay, using pressure from George Airport, to estimate propagation speeds of the CTW. Depth-integrated (barotropic) currents were calculated by weighted averaging of current velocities for each depth bin height (0.2 m–0.3 m) in the ADCP data and each grid cell height in the numerical model.

3. Results

3.1. Wind and model skill evaluation

Correlation coefficients (r) and relative bias (with respect to the modelled winds) in general wind velocity between the Automatic Weather Station (AWS) wind data from the South African Weather Service (SAWS) and the closest georeferenced grid cell in the CFSv2 dataset (Fig. 4) revealed a good correlation for most stations, with an average correlation of 0.83 ($p < 0.05$) (results summarised in Table 2). Relative bias for wind speeds were within 20% for most stations. The exact reasons behind the relatively poor correlation and high wind bias at the Plettenberg Bay AWS are uncertain, although likely due to its location very near a large cluster of aircraft hangars of the same height as the anemometer mount on a high wooded headland at an altitude of 138m.

Correlation coefficient, bias and Root-Mean-Square-Error (RMSE) were used along with the cost function χ , the ratio of RMSE against the standard deviation of the observations (Holt et al., 2005), to assess model performance to observations between 1 and 30 September 2014 (results summarised in Table 3, top). For the cost function χ , values less than 1 (RMSE smaller than the standard deviation of the observations) indicate that there is potential for the model to have predictive skill (Holt et al., 2005). Sea surface height had the overall best performance, with comparisons against the SANHO tide level recorder (Fig. 5c; Table 3) resulting in a correlation coefficient of 0.81, a mean bias of 0.013 m (σ (SD) = 0.015 m) (Mean SSH = 1.152 m), and χ of 0.62. Depth-averaged velocities showed less agreement. Zonal (eastward) and meridional (northward) current component velocities for Bird Island (Fig. 5a) had a relatively good correlation of 0.72 and 0.69 respectively, with χ indicating a better agreement in the zonal component (0.72) compared to the meridional component (0.88). A complex correlation estimates that the phase angle of the model data is rotated 17.7° counter-clockwise relative to the instrumentation data, with a correlation coefficient of 0.89. Cape Recife (Fig. 5b) performed the worst with regards to the zonal component velocities, with a correlation of 0.36 and χ of 1.05. The meridional component velocities performed moderately better with a correlation of 0.66 and χ of 0.85, although a positive bias in the model at higher southward velocities is evident (Fig. 5a). The site is directly to the east of a major headland oriented perpendicular to southwesterly winds, resulting in relatively small and stochastic flow patterns during southwesterly winds and ultimately leading to a poor representation of zonal velocities in the model (Fig. 8a,c). A complex correlation estimates that the phase angle of the model data is rotated 15.8° clockwise relative to the instrumentation data, with a correlation coefficient 0.78.

Model performance over the event itself, from 17–21 September

Table 2

Comparative analysis of NCEP CFSv2 10m wind and SAWS AWS wind for the period 1 January 2011 to 31 December 2015. Stations in the SANL3 study domain highlighted in bold. Correlation coefficient (r) and relative bias (CFSv2 wind velocity over AWS) shown.

AWS Station	Location		Altitude (m)	r ($p < 0.05$)	Relative Bias
	Latitude	Longitude			
Cape Agulhas	-34.8262	20.0131	11	0.91	+97%
Plettenberg Bay	-34.0896	23.3259	138	0.54	+69%
Cape St Francis	-34.2122	24.8357	9	0.78	- 3.5%
Port Elizabeth	-33.9827	25.6138	60	0.94	+18.9%
Coega	-33.8050	25.6680	46	0.92	+10.9%
Bird Island	-33.8388	26.2861	3	0.9	+15%
Port Alfred	-33.5595	26.8809	84	0.91	+46%
East London	-33.0225	27.8199	149	0.88	+6.9%

Table 3

Model skill assessment between observed and modelled depth integrated current velocity and sea surface height for the month from 1 to 30 September 2014 (top) and for the event from 17 to 21 September 2014 (bottom). P-value derived from cross correlation (r) using the effective degrees of freedom (N_{eff}).

	N_{eff}	BIAS	r	p-value	RMSE	X
Month: 1–30 September 2014						
Cape Recife (A1) Eastward Current (m/s)	47.5	0.013	0.36	0.006	0.062	0.96
Cape Recife (A1) Northward Current (m/s)	31.4	-0.081	0.66	<0.001	0.180	0.85
Bird Island (A2) Eastward Current (m/s)	19.2	-0.071	0.72	<0.001	0.213	0.72
Bird Island (A2) Northward Current (m/s)	27.7	-0.043	0.69	<0.001	0.093	0.88
Port Elizabeth Harbour (D1) Sea Level (m)	16.2	0.013	0.81	<0.001	0.076	0.62
Event: 17–21 September 2014						
Cape Recife (A1) Eastward Current (m/s)	6.3	0.033	0.54	0.12	0.069	1.11
Cape Recife (A1) Northward Current (m/s)	5.3	-0.066	0.80	0.03	0.126	0.71
Bird Island (A2) Eastward Current (m/s)	3.0	0.029	0.90	0.09	0.203	0.46
Bird Island (A2) Northward Current (m/s)	9.2	0.151	0.41	0.13	0.151	1.22
Port Elizabeth Harbour (D1) Sea Level (m)	2.6	0.023	0.95	0.09	0.059	0.34

2014 (results summarised in Table 3, bottom), fared slightly worse. Given the consistent nature of the CTW and its dominance on the variability in currents and sea level during the event itself, this inevitably results in lower effective degrees of freedom (N_{eff}) which makes significant correlations within the 95% confidence interval challenging. Cape Recife eastward currents and Bird Island northward current correlations fell well outside the 95% confidence interval. However, Cape Recife northward currents, Bird Island eastward currents, and Port Elizabeth Harbour sea level did show significant correlations within the 90% confidence interval. Fortunately, these are the key parameters used in the forthcoming assessments, with Cape Recife northward currents and Bird Island eastward currents most closely aligning with the along-shore direction.

3.2. The regional ocean response to a large wind event

Within the study domain, the southwesterly wind event began during the evening of 17 September 2014 following a northeasterly wind event and persisted for a total of 58 h (2.5 days). Hourly average wind speeds measured at the Port Elizabeth Airport AWS varied between 5.6 m/s and 15.7 m/s, with an average of 9.6 m/s over the entire duration of the event (Fig. 3b). The peak wind speed of 15.7 m/s (near gale) occurred on 19 September at 11h00. The wind event was strongly associated with a large fluctuation in sea level with an amplitude of 45 cm measured at the SANHO tide level recorder at the Port Elizabeth Harbour (Fig. 3c). The mean water level rose from 1.14 m to 1.59 m over a period of 42 h, reaching its peak at 04h00 on 19 September 2014, with a similar response observed in the SANL3 model (Fig. 3c). There is strong evidence for a CTW, given that there was a sudden reversal in depth integrated alongshore currents which increased significantly in velocity in tandem with the rising water level (Fig. 9). Examining tide level records, the CTW can be seen to originate from the west coast, first recorded at the Port Nolloth tide gauge and then propagating around southern Africa in a typical anti-clockwise fashion (Fig. 7a). The wave amplitude increased significantly along the south coast before dissipating near East London

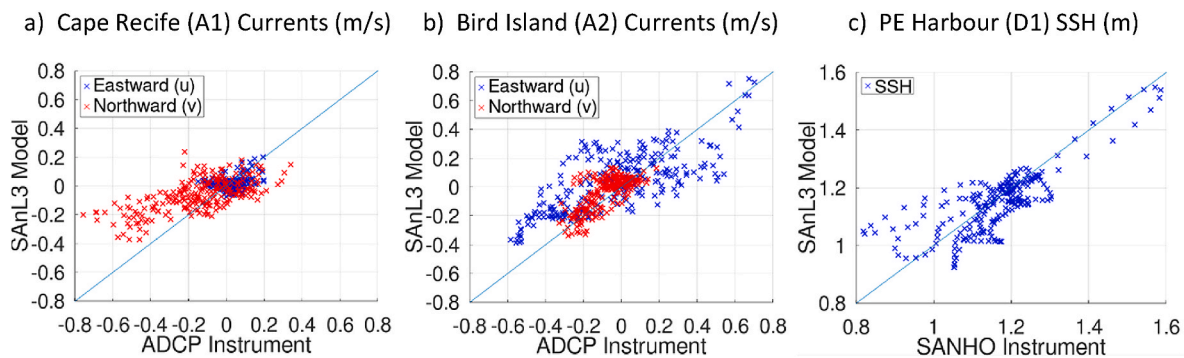


Fig. 5. Scatter plots of (a) the SANL3 model depth integrated currents against SAEON ADCP moorings at Cape Recife (A1) and (b) Bird Island (A2). (c) The SANL3 model sea surface height (SSH) against the SANHO tide level recorder in the Port Elizabeth Harbour (D1). Plot data from 1 to 30 September 2014. Negative values are southward/westward flow.

on the east coast in the same manner as described by Schumann and Brink (1990) and Schumann (2013). The wave was associated with winds generated by an eastward propagating low-pressure atmospheric system to the south of the country (shown for the CFSv2 model data in Fig. 6), evident by high zonal winds occurring in tandem with a large change in air pressure in the Mossel Bay and Port Elizabeth AWS (Fig. 7b,c,d). Using the switch in zonal wind direction to determine the propagation speed of the wind system, averaging this change between AWS stations from Plettenberg Bay to Port Alfred, a figure of 8.2 m/s is attained. The peaks in pressure corrected sea level records between Mossel Bay and Port Elizabeth occurred exactly 12 h apart (Fig. 7b), which indicates a wave propagation speed of approximately 7.5 m/s, matching that calculated by Schumann and Brink (1990) for the same region. Since the phase speed of the wind system is close to the typical free wave propagation speed of 8 m/s, the large amplitude CTW that is generated can be attributed to resonance effects (Allen and Denbo 1984; Schumann and Brink 1990).

The ocean response to the wind event was captured by the SAEON ADCP moorings at Cape Recife and Bird Island. The alongshore current at Cape Recife (meridional rotated 23° anti-clockwise), which is usually dominated by southward flow (Fig. 8a), underwent a barotropic reversal shortly after the arrival of the leading edge of the wave at 12h00 on 17 September 2014 (Fig. 9b,d). The northward flow lasted for approximately 23 h before mostly resuming to a southward flow just prior to the peak of the wave. At the Bird Island mooring, the alongshore current (zonal rotated 20° clockwise, according to the isobath contours) saw a relatively quick barotropic current reversal that took place from the onset of the wave, lasting approximately 60 h (Fig. 9b,e). The current reversal occurred within 1 h to the arrival of the southwesterly wind event, although it was a full 2 h ahead of the current reversal seen at the Cape Recife mooring. For the Bird Island ADCP, current reversal from the surface (5m) to 20m depth occurred within approximately 2 h and 20 min, with reversal to full depth (5m to 35m) occurring within approximately 3 h and 40 min. At Cape Recife, current reversal to full depth (5m to 22m) was far quicker, occurring within the 30 min sampling interval of the ADCP. After the establishment of currents to full depth, current structures were essentially barotropic until the Bird Island currents quickly returned to their pre-CTW state within 40 min, with Cape Recife currents becoming more stochastic prior to returning to their pre-CTW state within 4 h.

The wave and subsequent response in alongshore current was well represented in the numerical model (Fig. 9f,g,h). An approximate 3-h delay in the barotropic response in alongshore currents at Bird Island, compared to the ADCP mooring, was noted (Fig. 9e,j). Maximum depth integrated current speeds near the peak of the wave were exceptionally close between the ADCP observations and the numerical model. At Bird Island, eastward flows peaked at 0.77 m/s and 0.72 m/s for the ADCP and SANL3 model respectively (Fig. 9c,h; green plot). At Cape Recife,

northward flows peaked at 0.17 m/s and 0.16 m/s for the ADCP and SANL3 model respectively (Fig. 9c,h; red plot).

3.3. Examination of the event in the SANL3 models

Within the reference (SANL3 with wind) model, shortly after the preceding sea level trough (referenced as T0) at T0 + 0h (12h00 on 17 September 2014), eastward currents are quickly established after the onset of the southwesterly wind (Fig. 9). Current reversals occur within approximately 3 h between each assessment station (Fig. 10b–f), with circulation in the bays switching direction from counter-clockwise to clockwise (Fig. 11: T0 + 15h). This switch occurs approximately 6 h after the start of the wave (T0 + 0h) and is evident as a reversal of the flow from southward to northward at the Cape Recife (A1) ADCP mooring (Fig. 9d,i). Depth integrated current velocities peak at T0 + 30h (18h00 on 18 September 2014) (Fig. 10b), with a region of very high current velocities seen over a large area south of Cape St Francis (Fig. 11 left: T0 + 30h). An inverse relationship between the amplitude of the wave and the strength of the current reversals is evident (Table 4). The smallest wave height and strongest currents occur off Cape St Francis (B1), with the wave amplitude increasing as it passes offshore of Cape Recife (B2), Bird Island (B3) and Port Alfred (B4). This coincides with a progressive decline in peak wind speed at each station. Peak current velocities progressively decrease as the wave travels to the east, although the duration of each current reversal event is similar. The circulation in the two bays switches back to counter-clockwise very shortly after the peak of the wave at T0 + 30h, which was captured at the Cape Recife (A1) ADCP mooring as a current reversal back to southward flow (Fig. 9d,i). Nearshore current velocities begin to decrease steadily after T0 + 45h as surface winds slow and the wave begins to move out of the domain, although strong north-eastward flows are still present over the deeper portions of the shelf south of Cape St Francis and Cape Recife (Fig. 11 left: T0 + 45h). The counter-clockwise circulation patterns in St Francis and Algoa Bay become firmly established, with the near-shore currents having returned to south-westward flows (Fig. 10b–f) and residual north-eastward flows in the offshore shelf areas as the domain enters the post-CTW state at midnight on 20 September 2014 (Fig. 11 left: T0 + 60h).

An examination of the circulation in the SANL3 no-wind model during the passage of the CTW reveals similar patterns to the SANL3 reference model (Figs. 11 and 10). As expected, removal of surface forcing results in the wave progressively losing amplitude more rapidly as it travels to the north-east compared to the reference model (Table 4, Fig. 10m). At Port Alfred (B4), located past a sudden decrease in the continental shelf width to the east of Algoa Bay, the CTW amplitude increases with a slightly greater lag in the wave peak compared to the other stations. Currents are generally weaker in the no-wind model, given the absence of surface wind stress, with the flow over the shelf

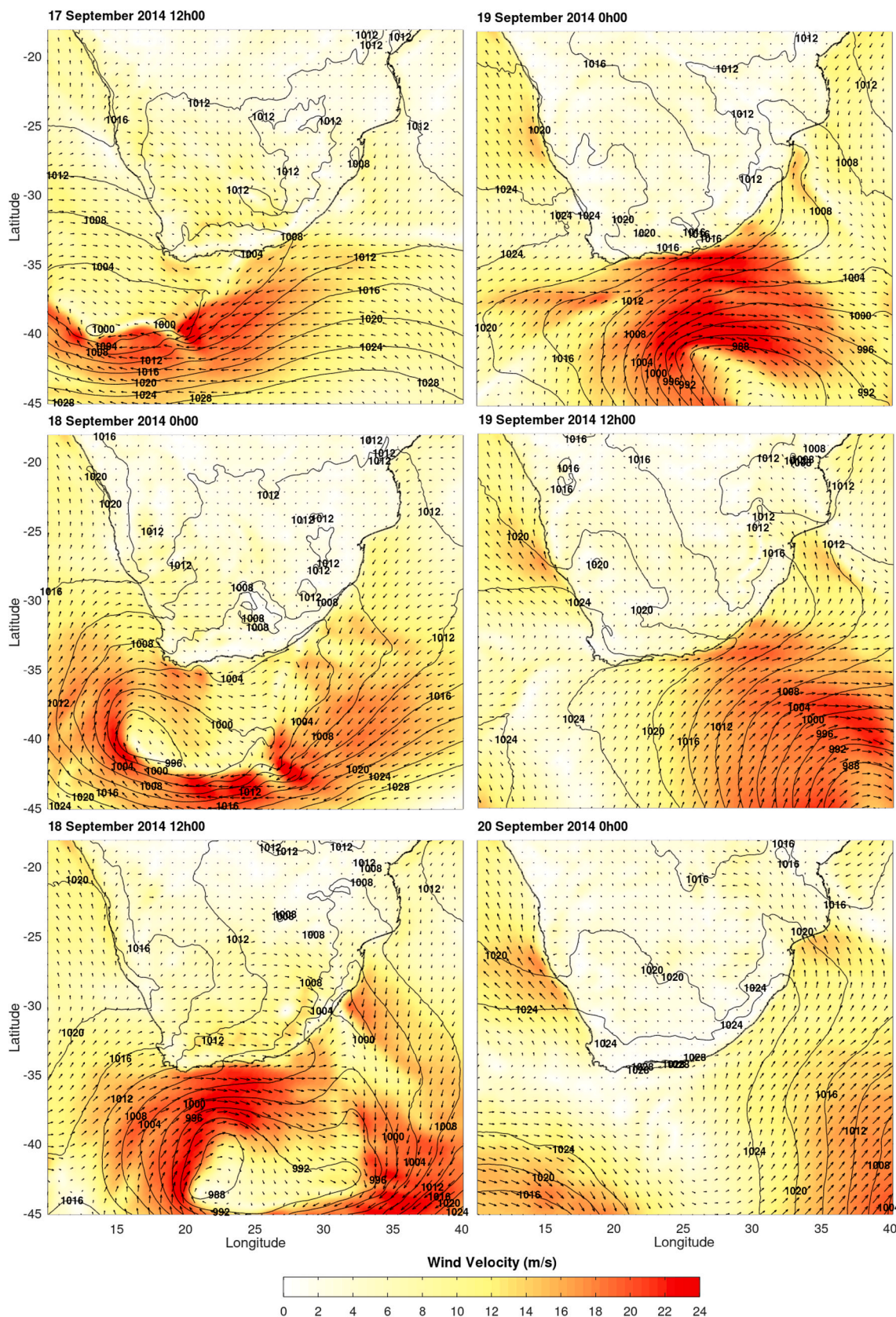


Fig. 6. CFSv2 Sea level pressure isobars (mb), wind direction (vectors) and wind velocity (shading) showing the progression of the low-pressure system and associated winds from 17 September 2014 12h00 to 20 September 2014 0h00.

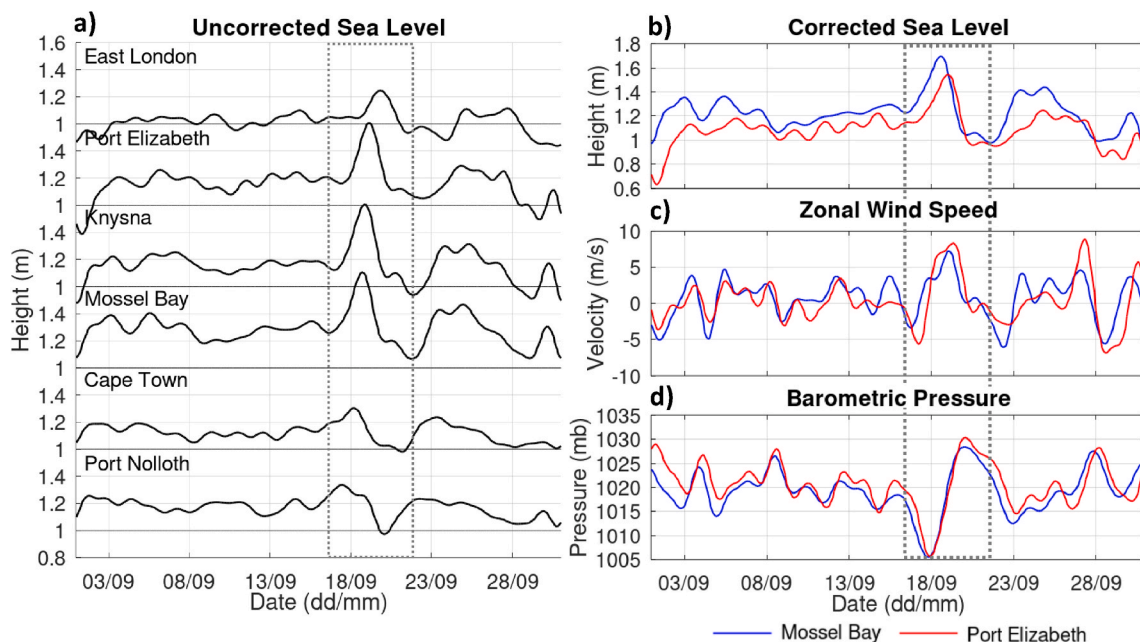


Fig. 7. (a) Uncorrected SANHO tide level records from Port Nolloth on the west coast of South Africa (bottom) to East London on the east coast (top). (b) Pressure corrected sea level, (c) zonal wind speed (positive eastward) and (d) barometric pressure for the Mossel Bay SAWS AWS (blue) and Port Elizabeth SAWS AWS (red). Dates shown from 1 to 30 September 2014. Coastal trapped wave event between 17 and 22 September 2014 highlighted with grey dashed box.

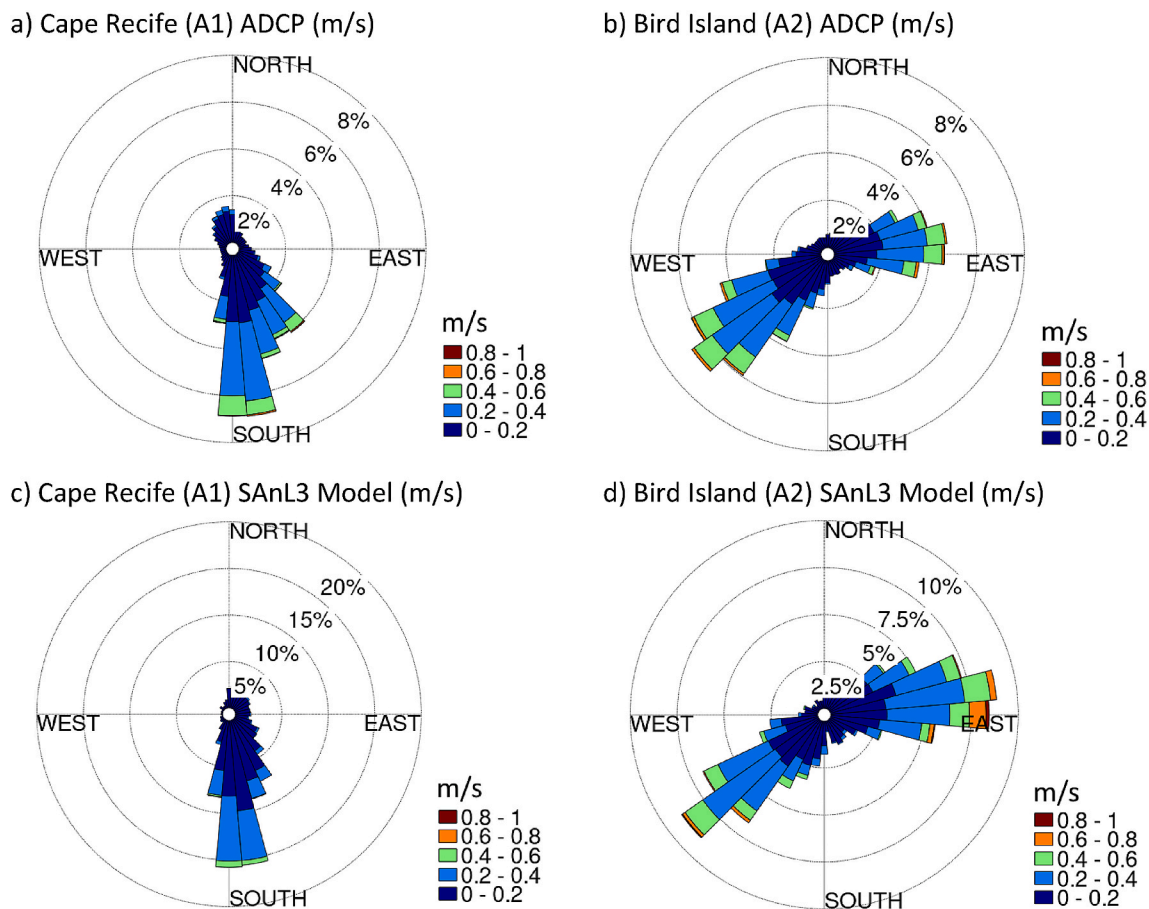


Fig. 8. Depth averaged (from surface to bottom) current rose for Cape Recife (A1) and Bird Island (A2) ADCP (a,b) and SANL3 Model in corresponding locations (c,d) from 1 January 2011 to 31 December 2015.

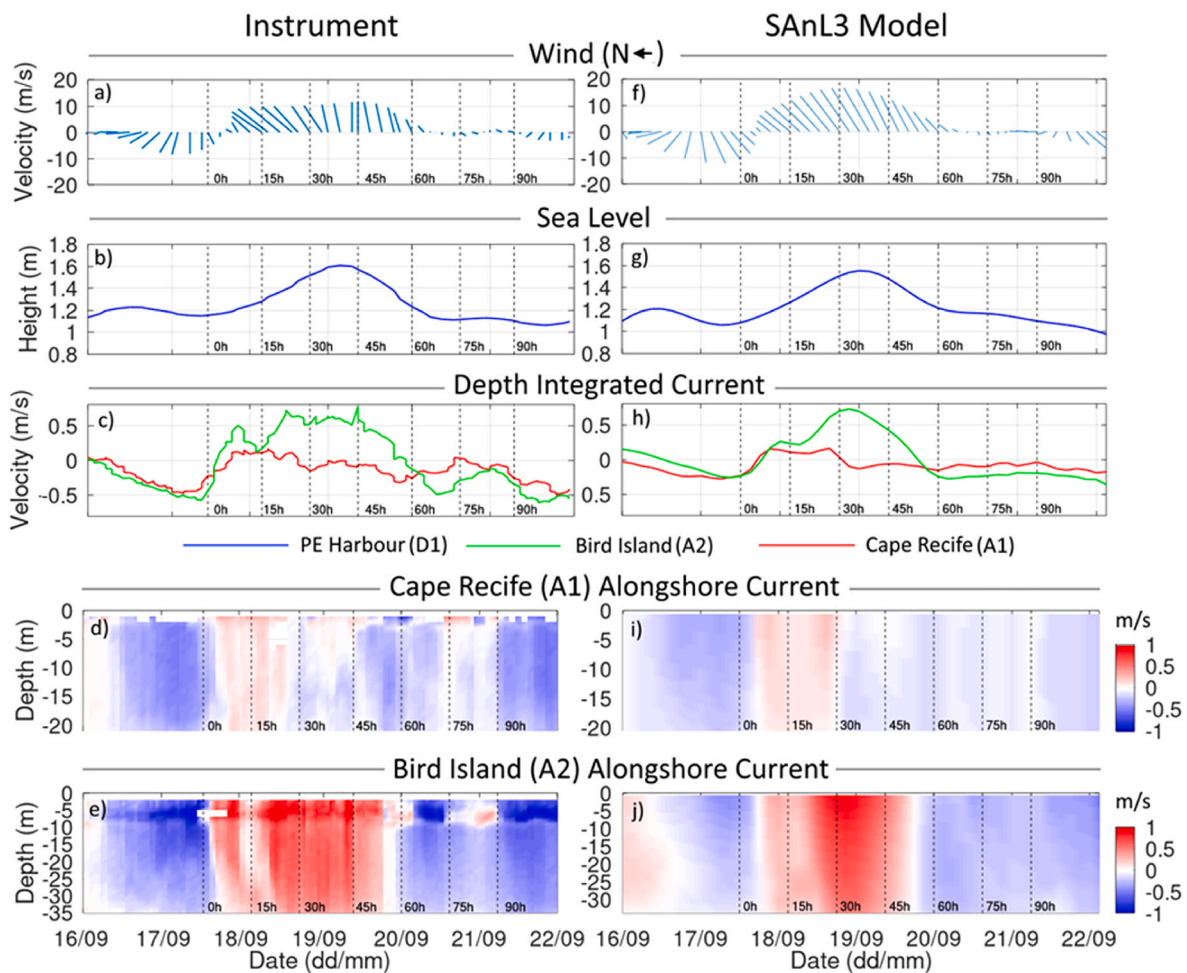


Fig. 9. The southwesterly wind event of 17 September 2014, with dashed lines showing time in 15h increments from the onset of the event (denoted by the preceding shelf wave sea level trough) at $T_0 + 0h$ (12h00 on 17 September 2014). Left panels (a–e) from *in situ* instrumentation, and right panels (f–j) from the closest matching grid cell location in the numerical models. (a,f) Wind at the Port Elizabeth Airport (Oriented northward to the left). (b,g) Sea level at the Port Elizabeth Harbour. (c,h) Depth-integrated alongshore current at Cape Recife (A1) and Bird Island (A2). (d,i) Alongshore current at Cape Recife and (e,j) Bird Island. Alongshore current oriented positive northward (CR (d,i))/eastward (BI (e,j)).

driven by the bulk displacement of water as the CTW passes. Peak current velocities become progressively weaker to the east, with the average barotropic velocity 18% less than the reference model (Table 4, Fig. 10n). This indicates that the water displacement caused by the CTW itself contributes significantly to the net flow observed during the strong southwesterly wind event.

3.4. Along-shelf transport, volume displacement and wave period

The modelled along-shelf transport across the transect C1 between Cape Recife and the shelf break (Fig. 2) during the event is shown in Fig. 12. Considering only the eastward flow, during the passage of the CTW a mean of 1.94Sv (1.59Sv) with a peak of 3.54Sv (2.92Sv) was reached, resulting in an eastward displacement of $335.2 \times 10^9 \text{ m}^3$ ($275.0 \times 10^9 \text{ m}^3$) for the reference (no-wind) model. In this case, the no-wind model run accounts for 82% of the eastward displacement, with the largest difference in transport between the reference and no-wind model seen just prior to the peak of the CTW at $T_0 + 30h$ (Fig. 12d). Examining cumulative volume displacement, i.e., the difference between the eastward and westward movement of the water mass, integrating from the preceding sea level trough of the CTW at $T_0 + 0h$ to the subsequent sea level trough of the CTW at $T_0 + 90h$ yields a net displacement to the east of $153.3 \times 10^9 \text{ m}^3$ ($93 \times 10^9 \text{ m}^3$) in the reference model (no-wind) model. This indicates that the volume displacement has not yet completed a full

cycle and thus may not be a true reflection of the actual wave period. If the start of the wave is instead taken as the zero-crossing point of transport across the C1 transect prior to the event, which occurs on 16 September 2014 at 0h00 ($T_0 - 36h$), then integrating from this point finds that the volume displacement completes a full cycle at $T_0 + 114h$ (150h after zero-crossing) for the reference model and $T_0 + 105h$ (141h after zero-crossing) for the no-wind model (Fig. 12c).

4. Discussion

A protracted southwesterly wind event lasting approximately 45h and reaching a peak hourly average of 15.7 m/s occurred between 17 and 20 September 2014, with a substantial response in sea level and circulation patterns captured by *in situ* sea level and ADCP moorings within Algoa Bay. A $dx \sim 1 \text{ km}$ ROMS numerical model, forced on the surface using hourly CFSv2 wind data, was able to reproduce the characteristics of the ocean response.

The prevailing southwesterly wind blowing in an approximately along-shelf direction, would be expected to result in onshore Ekman transport and subsequent sea-level set-up near the coastal boundary (Lentz and Fewings 2012). However, when considered with pressure corrected tide level records from stations to the west, it is evident that this response is also governed by the passage of lowest CTW mode, the characteristics of which were similar to that described by Goschen et al.

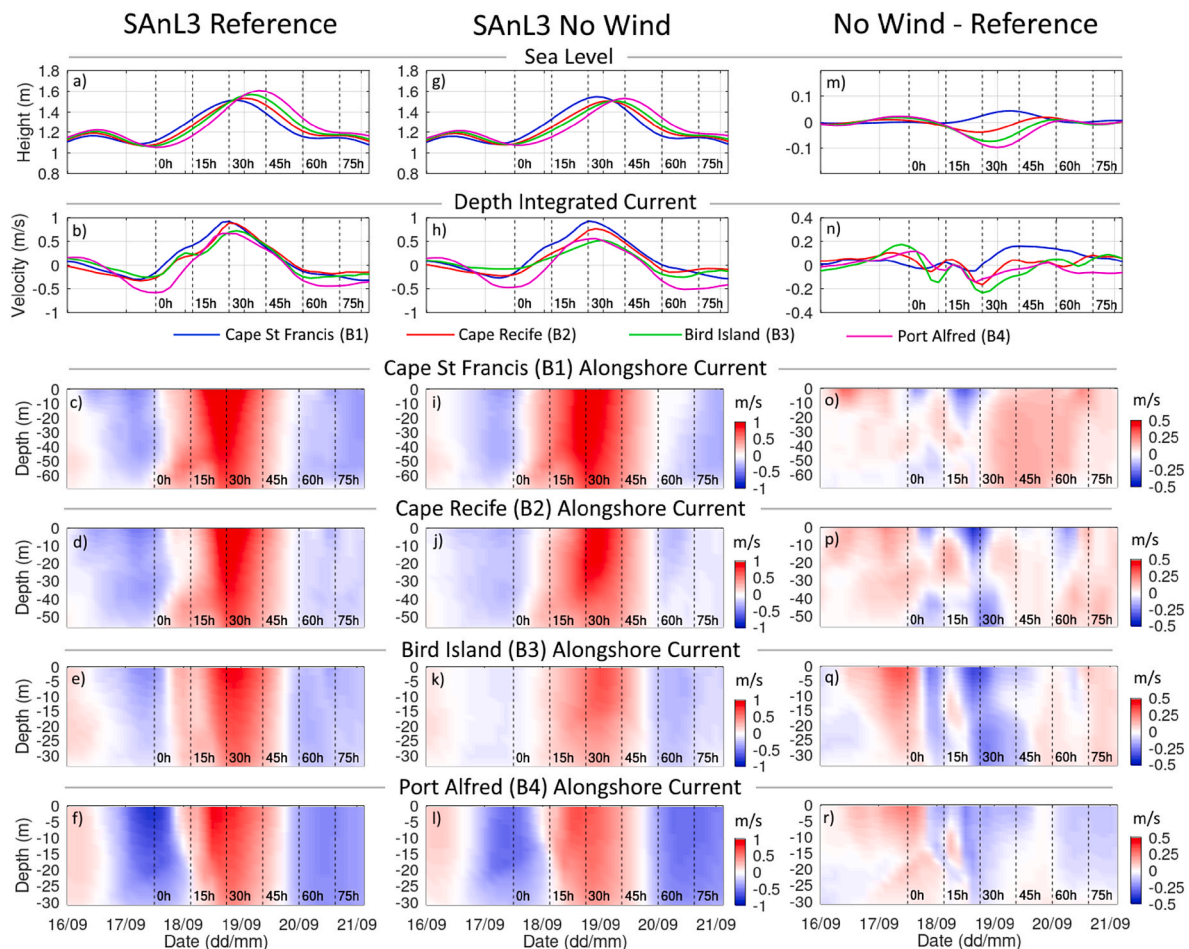


Fig. 10. Sea level, depth integrated current, and alongshore currents from 17 to 21 September 2014 from stations B1, B2, B3, and B4 (see Fig. 2) in the SANL3 reference model (a–f), SANL3 no wind model (g–l), and the difference between the no wind model and the reference model (m–r). Alongshore current oriented positive eastward/northward.

(2012) after capturing a CTW of similar magnitude at their study site off Bird Island on 3 February 2009. Within the reference model, the peak amplitude of the CTW increases despite a decrease in wind speeds as it travels eastward (Table 4, Fig. 10a). Within the no-wind model the shelf wave height remains relatively similar across all stations (B1 to B4). Although the observed wave height may be influenced by the station depth gradually decreasing toward the east, when considering a progressively narrowing shelf in the direction of wave propagation coupled with the conservation of wave energy, one would expect a similar effect of shelf width on increasing CTW amplitude and decreasing propagation speed as observed by Kitade and Matsuyama (2000) along the southeast coast of Honshu, Japan, and demonstrated by Maiwa et al. (2010) in a shelf modelling experiment around Tasmania and the eastern coast of Australia. This was also demonstrated by Rivas (2017), showing the drop in phase speed in relation to the narrowing of the shelf to be consistent with expected dynamical-mode calculations.

The omission of local wind forcing in the no-wind model demonstrates that remote forcing along the shelf to the west of the domain boundary at Oyster Bay can be a significant contributor to local circulation, particularly during strong wind events. This is predominantly governed by the passing CTW, and similar processes have been investigated and described in the local context along the southern African coastline (e.g. Jury et al., 1990; Schumann and Brink 1990) and in other regions (e.g., South-eastern Australian Coast - Church et al., 1986, Gulf of Mexico - Rivas 2017, South-west African coast - Junker et al., 2019, Fukushima coast - Kubota et al., 1981, South China Sea northern coast - Ding et al., 2012, West coast of India - Amol et al., 2012, 2018, Northern

portion of the California Current System - Engida et al., 2016). Apart from the Port Alfred (B4) station, full depth alongshore current reversals were recorded at all other SANL3 model stations within two model output time steps (6 h) of the change in wind direction (Fig. 10), with the ADCP's showing a strong full depth current reversal with a time lag of less than 4 h to the wind switch (Fig. 9). In an idealized sense, at this latitude (34° South) the establishment of the Ekman layer to its full depth would be expected to take approximately 10 h (as demonstrated analytically by Gill (1982) and Brink (1983)), indicating the period of time before the effects of wind at the surface affects currents throughout the entire water column. Goschen et al. (2012) found a 2.5-h phase lag between winds and surface currents at the Bird Island (A2) ADCP mooring, outside of any CTW activity. Sharp barotropic current reversals during the passage of CTW along the south coast were also noted by Schumann and Brink (1990). In case studies by Jury et al. (1990), it was found that the phase relationship between propagating wind systems and shelf waves along the west and south coast of South Africa was close, to the point of near-resonance, and that current reversals were primarily controlled by shelf waves which are in turn forced with the propagation of alongshore winds associated with coastal flows. The currents induced by the propagating atmospheric wind system and associated ocean shelf wave contribute to the transient along-shelf transport of shelf waters during such events, as seen in the SANL3 model shown in Fig. 12.

The offshore structure of the CTW is intriguing. Examining the depth-integrated current speeds as shown in Fig. 11, the strongest currents are seen to the south of Cape St Francis, with velocities exceeding 0.7 m/s

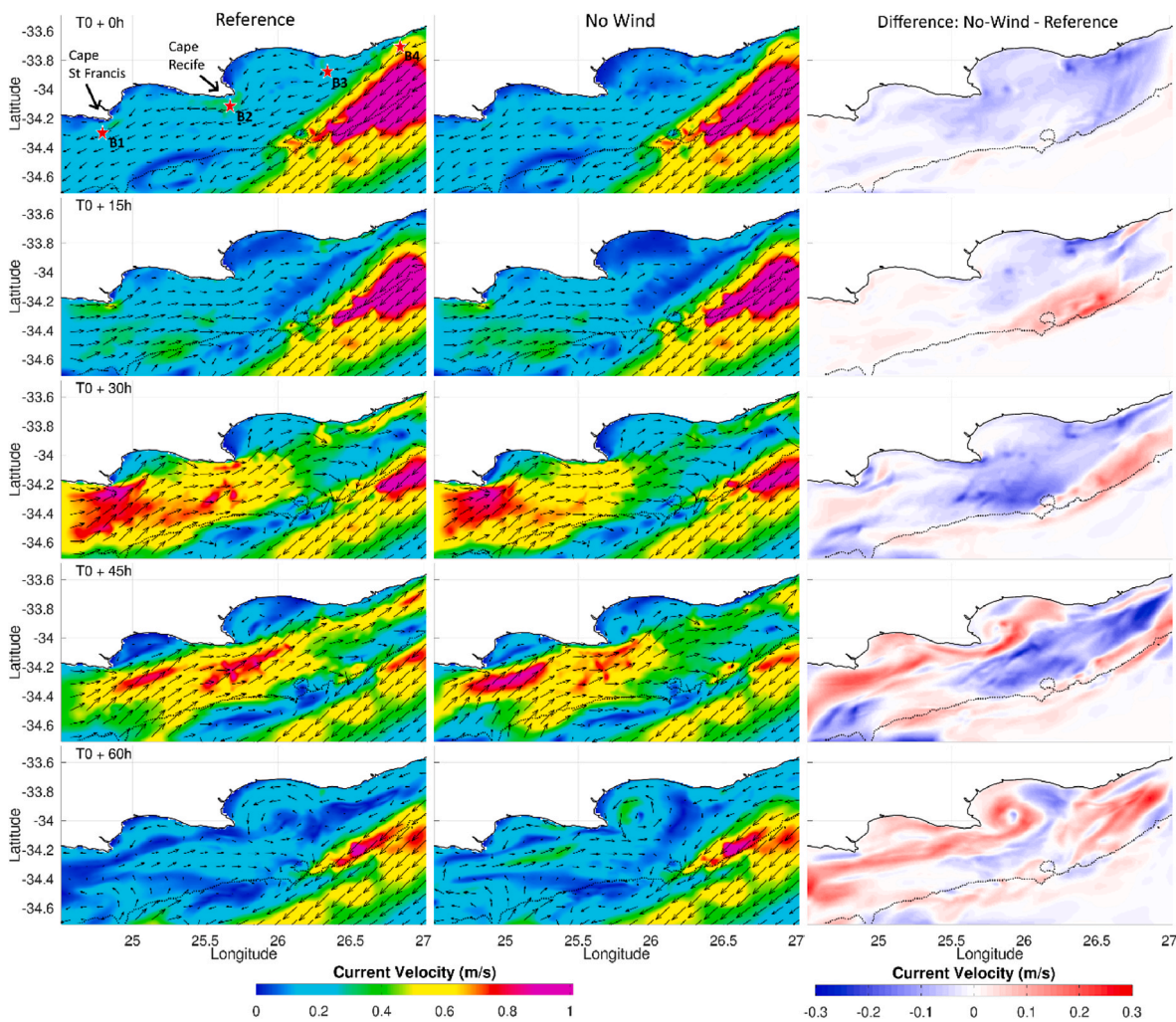


Fig. 11. Depth-integrated current direction (vectors) and velocity (shading) during the passage of the coastal trapped wave in the SANL3 reference model (left), the no wind model (middle), and the velocity difference between the no wind model and the reference model (right). T0 = 12h00, 17 September 2014. Dotted black line denotes the 200m isobath. B1,B2,B3, and B4 current assessment station locations shown top left.

Table 4

Peak wind speed (CFSv2), wave height, and depth-integrated eastward/north-eastward alongshore current velocity at stations B1, B2, B3, and B4 for the reference and no wind SANL3 models.

Depth	Cape St Francis (B1)		Cape Recife (B2)		Bird Island (B3)		Port Alfred (B4)	
	65 m		55 m		35 m		30 m	
	Wind	No Wind	Wind	No Wind	Wind	No Wind	Wind	No Wind
Wind Max (m/s)	20.3	–	18.8	–	15.8	–	13.4	–
CTW Height (m)	1.51	1.54	1.53	1.5	1.57	1.5	1.61	1.53
Alongshore Current (m/s)	0.92	0.93	0.89	0.77	0.72	0.53	0.67	0.56

across most of the shelf width. It appears that, in this region, the Cape St Francis headland behaves as a choke point, coinciding with a sudden narrowing of the shelf approaching from the west (see Fig. 1b), thereby constraining the wave as it propagates eastward into the domain. This will likely remove some energy from the wave (evident up to the peak of the wave at T0+30h in Fig. 10o,p and the no-wind plot of Fig. 11), indicating this to be a potential region of wave scattering into higher modes (see Wilkin and Chapman 1990). The current structures over the shelf off Cape Recife indicate that this headland then acts as a second choke point, possibly scattering the wave further. This is pure hypothetical conjecture, given the inherent difficulty of assessing wave scattering in general, but it does open curious prospects when one considers how higher modes may interact with the south-westward

flowing AC, thereby contributing to its dynamics. Brunner et al. (2019) make an interesting proposal that backscattering due to a narrowing shelf and separation of a major boundary current, in this case the Gulf Stream, lead to the enhancement of southward travelling CTW near Duck, North Carolina, before dissipating to the south. It is possible that a similar mechanism is at play here, but further work is still needed to fully understand the influence of friction and scattering on the generation and dampening of higher mode waves (Clarke and Van Gorder 1986; Brunner et al., 2019).

Comparison of water transport between the reference and no wind model across the C1 transect off Cape Recife suggests that an estimated 82% of the transient eastward transport flux is due primarily to remote wind forcing to the west of the region. This displaces a considerable

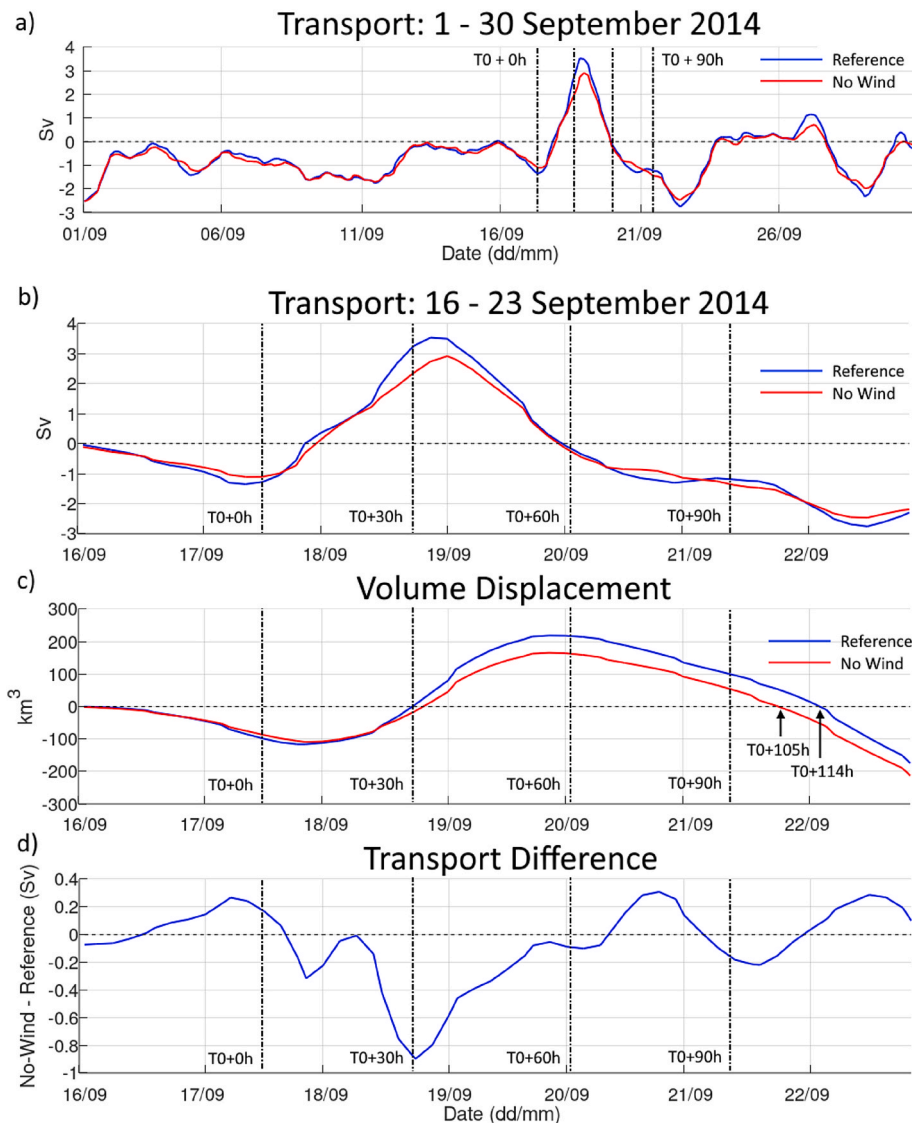


Fig. 12. Along-shelf volume transport across transect C1 between Cape Recife and 10 km from the inshore front of the AC. a) Transport for the month of September 2014. b-d) Assessment during the passage of the CTW from 16–23 September 2014: b) Transport, c) cumulative volume displacement (from transport zero-crossing point on 16 September 2014 0h00 (T0 - 36h). Time of complete displacement cycle shown by arrows), and d) transport difference between the runs (scaled according to the range of difference).

amount of water to the east of Cape Recife, to the tune of $335.2 \times 10^9 \text{ m}^3$ ($275.0 \times 10^9 \text{ m}^3$), which is balanced (i.e., completes a full wave cycle) over a period of 150h (141h) after the initial zero-crossing point of the transport flux for the reference (no-wind) model. If one considers the approximate volume of Algoa Bay and St Francis Bay as $55 \times 10^9 \text{ m}^3$ and $37 \times 10^9 \text{ m}^3$ respectively (conservatively estimated using GIS, with an average depth of 40m estimated from GEBCO bathymetry, and the boundary from Cape Recife to Cape Padrone, and Cape St Francis to Cape Recife, respectively), then the eastward displacement constitutes some 364% of the combined volume of the two bays.

The time frame between the transport zero-crossing point (T0 - 36h) and the apparent sea level trough of the CTW (T0 + 0h, a few hours prior to the zero wind isoline) was close to that observed by Jury et al. (1990) when measuring the typical time between shelf wave trough passage and the zero wind isoline. If we assume a symmetric linear wave, then this lends support to the notion that the transport zero-crossing point in this case indicates the true trough of the CTW, which in turn indicates that the volume displacement cycle time of 150h may be a closer estimation of the true period of the wave.

5. Conclusion

In situ instruments and high resolution ROMS model data were used

to investigate the effects of an eastward travelling wind system on sea level and circulation responses in the shelf and bays on the eastern Agulhas Bank. Measurements at tide level recorders across the western and southern coasts of South Africa indicated that the event was associated with an eastward travelling CTW that passed through the study region. Sudden alongshore current reversals to the full depth were seen at the ADCP sites to the south-west of Bird Island and to the east of Cape Recife, with the ROMS model showing this current reversal also occurring south of Cape St Francis and south of Cape Recife, with particularly strong currents developing here at the peak of the CTW ($>1 \text{ m/s}$). The omission of local wind forcing in the model demonstrated that the CTW can carry a significant amount of energy into the domain from remote forcing along the shelf to the west of Oyster Bay. An along-shelf transport assessment over a cross-shelf transect south of Cape Recife illustrated that this remote wind forcing can be responsible for an estimated 82% of the eastward movement of the water mass during the event. It was also shown that it takes an estimated 150h for the displacement of the water mass to complete a full cycle, which may be a better reflection of the actual wave period and the time it takes for the system to return fully to its previous state after the passage of the wave.

The substantial along-shelf movement of water coupled with the changes in circulation patterns within the bays highlight the importance of such wind events on governing water exchange between the bays and

the shelf. Such voluminous displacements and long cycle times would have significant implications for regional marine biota, particularly sessile reef habitats, and the effects of climate change on local pressure and wind systems could alter the characteristics of these marine environments by enhancing or diminishing the movement and exchange of shelf waters. This will most certainly apply to other shelf regions that experience CTW activity of a similar nature, such as the southeast and southwest coast of Australia. Although the characteristics will undoubtedly be different, the effects of CTW should be markedly similar, in turn allowing for inferences to be made regarding their impact on coastal marine systems under a changing global climate.

Declaration of competing interest

The authors declare the following financial interests/personal relationships which may be considered as potential competing interests: Dylan F. Bailey reports a relationship with Bayworld Museum Complex that includes: employment.

Acknowledgements

We are grateful to the South African Weather Service (SAWS), the South African Environmental Observation Network's (SAEON) Elwandle Node, and the South African National Hydrographers Office (SANHO) for providing the invaluable weather, ocean sensor, and tide gauge data respectively for this study. This research was supported by a Deans PhD Bursary from the Department of Oceanography at the Nelson Mandela University, Port Elizabeth.

References

- Adams, J.K., Buchwald, V.T., 1969. The generation of continental shelf waves. *J. Fluid Mech.* 35, 815–826.
- Allen, J.S., Denbo, D.W., 1984. Statistical characteristics of the large-scale response of coastal Sea Level to atmospheric forcing. *J. Phys. Oceanogr.* 14, 1079–1094.
- Amol, P., Shankar, D., Aparna, S.G., Shenoi, S.S.C., Fernando, V., Shetye, S.R., Mukherjee, A., Agarvadekar, Y., Khalap, S., Satelkar, N.P., 2012. Observational evidence from direct current measurements for propagation of remotely forced waves on the shelf off the west coast of India. *J. Geophys. Res.: Oceans* 117, 1–15.
- Amol, P., Vijith, V., Fernando, V., Pednakar, P., Singh, J., 2018. Impact of local and remote winds on the shelf circulation off the central west coast of India. *Ocean Dynam.* 68, 1607–1623.
- Bachèlery, M Lou, Illig, S., Rouault, M., 2020. Interannual coastal trapped waves in the Angola-Benguela upwelling system and Benguela Niño and Niña events. *J. Mar. Syst.* 203.
- Backeberg, B.C., Johannessen, J.A., Bertino, L., Reason, C.J., 2008. The greater Agulhas Current system: an integrated study of its mesoscale variability. *J. Oper. Oceanogr.* 1, 29–44.
- Bailey, D., 2020. Ocean Dynamics of the Shelf and Bays of the Eastern Agulhas Bank: A Process-Oriented Numerical Modelling Study. Nelson Mandela University.
- Beal, L.M., Eliport, S., Houk, A., Leber, G.M., 2015. Capturing the transport variability of a western boundary jet: results from the Agulhas current time-series experiment (ACT)*. *J. Phys. Oceanogr.* 45, 1302–1324.
- Bremner, J., 1983. Properties of logarithmic spiral beaches with particular reference to Algoa Bay. In: McLachlan, A., Erasmus, T. (Eds.), *Sandy Beaches as Ecosystems*. Junk, The Hague, pp. 97–113 (Developments in Hydrobiology 19).
- Brink, K.H., 1983. The near-surface dynamics of coastal upwelling. *Prog. Oceanogr.* 12, 223–257.
- Brink, K.H., 1990. On the damping of free coastal-trapped waves. *J. Phys. Oceanogr.* 20, 1219–1225.
- Brink, K.H., 2006. Coastal Trapped Waves with Finite Bottom Friction. pp. 2–3, 2005.
- Brouwer, S.L., Griffiths, M.H., Roberts, M.J., 2010. Adult movement and larval dispersal of *Argyrosoma argyrosoma* (Pisces: Sparidae) from a temperate marine protected area. *Afr. J. Mar. Sci.* 37–41.
- Brunner, K., Rivas, D., Lwiza, K.M.M., 2019. Application of classical coastal trapped wave theory to high-scattering regions. *J. Phys. Oceanogr.* 49, 2201–2216.
- Church, J.A., Freeland, H.J., Smith, R.L., 1986. Coastal-trapped waves on the East Australian continental shelf part I: propagation of modes. *J. Phys. Oceanogr.* 16, 1929–1943.
- Clarke, A.J., Brink, K.H., 1985. The response of stratified, frictional flow of shelf and slope waters to fluctuating large-scale, low-frequency wind forcing. *J. Phys. Oceanogr.* 15, 439–453.
- Clarke, A.J., Van Gorder, S., 1986. A method for estimating wind-driven frictional, time-dependent, stratified shelf and slope water flow. *J. Phys. Oceanogr.* 16, 1013–1028.
- Cucco, A., Quattrocchi, G., Zecchetto, S., 2019. The role of temporal resolution in modeling the wind induced sea surface transport in coastal seas. *J. Mar. Syst.* 193, 46–58.
- Ding, Y., Bao, X., Shi, M., 2012. Characteristics of coastal trapped waves along the northern coast of the south china sea during year 1990. *Ocean Dynam.* 62, 1259–1285.
- Durgadoo, J.V., Loveday, B.R., Reason, C.J.C., Penven, P., Biastoch, A., 2013. Agulhas leakage predominantly responds to the southern hemisphere Westerlies. *J. Phys. Oceanogr.* 43, 2113–2131.
- Egbert, G.D., Erofeeva, S.Y., 2002. Efficient inverse modeling of barotropic ocean tides. *J. Atmos. Ocean. Technol.* 19, 183–204.
- Engida, Z., Monahan, A., Ianson, D., Thomson, R.E., 2016. Remote forcing of subsurface currents and temperatures near the northern limit of the California Current System. *J. Geophys. Res.: Oceans* 121, 7244–7262.
- Gaspar, P., Ponte, R.M., 1997. Relation between sea level and barometric pressure determined from altimeter data and model simulations. *J. Geophys. Res. C Oceans* 102, 961–971.
- Gill, A.E., 1982. *Atmosphere-Ocean Dynamics*, first ed. edn. Academic Press.
- Gill, A.E., Schumann, E.H., 1974. The generation of long shelf waves by the wind. *J. Phys. Oceanogr.* 4, 83–90.
- Goschen, W., Schumann, E., Bernard, K., Bailey, S., Deyzel, S., 2012. Upwelling and ocean structures off Algoa Bay and the south-east coast of South Africa. *Afr. J. Mar. Sci.* 37–41.
- Goschen, W.S., Schumann, E.H., 1988. Ocean current and temperature structures in Algoa bay and beyond in November 1986. *S. Afr. J. Mar. Sci.* 7, 101–116.
- Haidvogel, D.B., Beckmann, A., 1999. *Numerical Ocean Modelling*. Imperial College Press.
- Harris, T.F.W., 1978. Review of coastal currents in southern African waters. *South Afr. Natl. Sci. Programmes* 30.
- Hermes, J.C., Reason, C.J.C., Lutjeharms, J.R.E., 2007. Modeling the variability of the greater Agulhas current system. *J. Clim.* 20, 3131–3146.
- Holt, J.T., Allen, J.L., Proctor, R., Gilbert, F., 2005. Error quantification of a high-resolution coupled hydrodynamic-ecosystem coastal-ocean model: Part 1 model overview and assessment of the hydrodynamics. *J. Mar. Syst.* 57, 167–188.
- Hutchinson, K., Beal, L.M., Penven, P., Anson, I., Hermes, J., 2018. Seasonal phasing of Agulhas current transport tied to a baroclinic Adjustment of near-field winds. *J. Geophys. Res.: Oceans* 7067–7083.
- Huthnance, J.M., 1975. On trapped waves over a continental shelf. *J. Fluid Mech.* 69, 689–704.
- Junker, T., Mohrholz, V., Schmidt, M., Siegfried, L., van der Plas, A., 2019. Coastal trapped wave propagation along the southwest African shelf as revealed by moored observations. *J. Phys. Oceanogr.* 49, 851–866.
- Jury, M., MacArthur, C., Reason, C., 1990. Observations of trapped waves in the atmosphere and ocean along the coast of Southern Africa. *S. Afr. Geogr. J.* 72, 33–46.
- Kitade, Y., Matsuyama, M., 2000. Coastal trapped waves with several day period caused by wind along the southeast coast of Honshu, Japan. *J. Oceanogr.* 56, 727–744.
- Krug, M., Swart, S., Gula, J., 2017. Submesoscale cyclones in the Agulhas current. *Geophys. Res. Lett.* 44, 346–354.
- Kubota, M., Nakata, K., Nakamura, Y., 1981. Continental shelf waves off the fukushima coast Part I: Observations. *J. Oceanogr. Soc. Jpn.* 37, 267–278.
- Lentz, S.J., Fewings, M.R., 2012. The wind- and wave-driven inner-shelf circulation. *Ann. Rev. Mar. Sci.* 4, 317–343.
- Lück-Vogel, M., Le Roux, A., Ludick, C., 2019. Green Book. The Impact of Climate Changes on Coastal Zones (Pretoria).
- Lutjeharms, J.R.E., Roberts, H.R., 1988. The natal pulse: an extreme transient on the Agulhas current. *J. Geophys. Res.* 93, 631–645.
- Lutjeharms, J.R.E., Boebel, O., Rossby, H.T., 2003a. Agulhas cyclones. *Deep Sea Res. Part II Top. Stud. Oceanogr.* 50, 13–34.
- Lutjeharms, J.R.E., Catzel, R., Valentine, H.R., 1989. Eddies and other boundary phenomena of the Agulhas Current. *Contin. Shelf Res.* 9, 597–616.
- Lutjeharms, J.R.E., Penven, P., Roy, C., 2003b. Modelling the shear edge eddies of the southern Agulhas Current. *Contin. Shelf Res.* 23, 1099–1115.
- Maiwa, K., Masumoto, Y., Yamagata, T., 2010. Characteristics of coastal trapped waves along the southern and eastern coasts of Australia. *J. Oceanogr.* 66, 243–258.
- Marchesiello, P., Debreu, L., Couvelard, X., 2009. Spurious diapycnal mixing in terrain-following coordinate models: the problem and a solution. *Ocean Model.* 26, 156–169.
- Marchesiello, P., McWilliams, J.C., Shchepetkin, A., 2001. Open boundary conditions for long-term integration of regional oceanic models. *Ocean Model.* 3, 1–20.
- Martínez, J.A., Allen, J.S., 2004a. A modeling study of coastal-trapped wave propagation in the Gulf of California. Part II: response to idealized forcing. *J. Phys. Oceanogr.* 34, 1332–1349.
- Martínez, J.A., Allen, J.S., 2004b. A modeling study of coastal-trapped wave propagation in the Gulf of California. Part I: response to remote forcing. *J. Phys. Oceanogr.* 34, 1313–1331.
- Mason, E., Molemaker, J., Shchepetkin, A.F., Colas, F., McWilliams, J.C., Sangrà, P., 2010. Procedures for offline grid nesting in regional ocean models. *Ocean Model.* 35, 1–15.
- National Oceanographic Data Center, 2013. NODC Standard Product: World Ocean Atlas 2009 (NCEI Accession 0094866). Temperature and Salinity. NOAA National Centers for Environmental Information. Dataset. <https://accession.nodc.noaa.gov/0094866>. (Accessed 16 July 2015).
- Nhantumbo, B.J., 2014. Sea Level Variability and Coastal Trapped Waves Around Southern Africa. University of Cape Town.
- Patrick, P., Strydom, N., Goschen, W., 2013. Shallow-water, nearshore current dynamics in Algoa Bay, South Africa, with notes on the implications for larval fish dispersal. *Afr. J. Mar. Sci.* 35, 269–282.
- Penven, P., Chang, N., Shillington, F., 2006a. Modelling the Agulhas current using SAFE (southern Africa experiment). *Geophys. Res. Abstr.* 8.

- Penven, P., Debreu, L., Marchesiello, P., McWilliams, J.C., 2006b. Evaluation and application of the ROMS 1-way embedding procedure to the central California upwelling system. *Ocean Model.* 12, 157–187.
- Pörtner, H.-O., Roberts, D.C., Masson-Delmotte, V., Zhai, P., Tignor, M., Poloczanska, E., Mintenbeck, K., Alegría, A., Nicolai, M., Okem, A., et al., 2019. IPCC Special Report on the Ocean and Cryosphere in a Changing Climate.
- Rivas, D., 2017. Wind-driven coastal-trapped waves off southern Tamaulipas and northern Veracruz, western Gulf of Mexico, during winter 2012–2013. *Estuar. Coast Shelf Sci.* 185, 1–10.
- Roberts, M.J., 2010. Coastal currents and temperatures along the eastern region of Algoa Bay, South Africa, with implications for transport and shelf-bay water exchange. *Afr. J. Mar. Sci.* 32, 145–161.
- Roberts, M.J., van der Lingen, C.D., Whittle, C., van den Berg, M., 2010. Shelf currents, lee-trapped and transient eddies on the inshore boundary of the Agulhas Current, South Africa: their relevance to the KwaZulu-Natal sardine run. *Afr. J. Mar. Sci.* 32, 423–447.
- Saha, S., Moorthi, S., Wu, X., Wang, J., Nadiga, S., Tripp, P., Behringer, D., Hou, Y.T., Chuang, H.Y., Iredell, M., et al., 2014. The NCEP climate forecast system version 2. *J. Clim.* 27, 2185–2208.
- Schumann, E.H., 1983. Long-period coastal trapped waves off the southeast coast of Southern Africa. *Continental Shelf Res.* 2, 97–107.
- Schumann, E.H., 1999. Wind-driven mixed layer and coastal upwelling processes off the south coast of South Africa. *J. Mar. Res.* 57, 671–691.
- Schumann, E.H., 2013. Sea level variability in South African estuaries. *South Afr. J. Sci.* 109, 1–7.
- Schumann, E.H., Brink, K.H., 1990. Coastal-trapped waves off the coast of South Africa: generation, propagation and current structure. *J. Phys. Oceanogr.* 20, 1206–1218.
- Schumann, E.H., van Heerden, I., 1988. Observations of Agulhas current frontal features south of Africa, October 1983. *Deep Sea Res. Part A, Oceanographic Research Papers* 35, 1355–1362.
- Schumann, E.H., Churchill, J.R.S., Zaayman, H.J., 2005. Oceanic variability in the western sector of Algoa Bay, South Africa. *Afr. J. Mar. Sci.* 27, 65–80.
- Shchepetkin, A.F., McWilliams, J.C., 2005. The regional oceanic modeling system (ROMS): a split-explicit, free-surface, topography-following-coordinate oceanic model. *Ocean Model.* 9, 347–404.
- Shikha, S., Valsala, V., 2018. Subsurface ocean biases in climate models and its implications in the simulated interannual variability: A case study for Indian Ocean. *Dyn. Atmos. Ocean.* 84, 55–74.
- Tao, W., Huang, G., Hu, K., Gong, H., Wen, G., Liu, L., 2016. A study of biases in simulation of the Indian Ocean basin mode and its capacitor effect in CMIP3/CMIP5 models. *Clim. Dyn.* 46, 205–226.
- Tedesco, P., Gula, J., Ménesguen, C., Penven, P., Krug, M., 2019. Generation of submesoscale frontal eddies in the Agulhas current. *J. Geophys. Res.: Oceans* 124, 7606–7625.
- Tilney, R.L., Nelson, G., Radloff, S.E., Buxton, C.D., 1996. Ichthyoplankton distribution and dispersal in the Tsitsikamma National Park marine reserve, South Africa. *S. Afr. J. Mar. Sci.* 17, 1–14.
- Wilkin, J.L., Chapman, D.C., 1990. Scattering of coastal-trapped waves by irregularities in coastline and topography. *J. Phys. Oceanogr.* 20, 396–421.
- Woodham, R., Brassington, G.B., Robertson, R., Alves, O., 2013. Propagation characteristics of coastally trapped waves on the Australian Continental Shelf. *J. Geophys. Res.: Oceans* 118, 4461–4473.